Synthesis and Properties of Poly(butylene terephthalate)/ Multiwalled Carbon Nanotube Nanocomposites Prepared by *In Situ* Polymerization and *In Situ* Compatibilization

Fangjuan Wu,[1,2] Guisheng Yang[2,3]

[1]*Department of Materials Science and Engineering, Fujian University of Technology, Fuzhou 350108, People's Republic of China*
[2]*Chinese Academy of Sciences Key Laboratory of Engineering Plastics, Joint Laboratory of Polymer Science and Materials, Institute of Chemistry, Chinese Academy of Sciences, Beijing 100190, People's Republic of China*
[3]*Shanghai Genius Advanced Materials Company, Limited, Shanghai 201109, People's Republic of China*

Received 10 January 2010; accepted 12 April 2010
DOI 10.1002/app.32625
Published online 30 June 2010 in Wiley InterScience (www.interscience.wiley.com).

ABSTRACT: A novel cyclic initiator was synthesized from dibutyl tin(IV) oxide and hydroxyl-functionalized multiwalled carbon nanotubes (MWNTs) and was used to initiate the ring-opening polymerization of cyclic butylene terephthalate oligomers to prepare poly(butylene terephthalate) (PBT)/MWNT nanocomposites. The results of Fourier transform infrared and NMR spectroscopy confirmed that a graft structure of PBT on the MWNTs was formed during the *in situ* polymerization; this structure acted as an *in situ* compatibilizer in the nanocomposites. The PBT covalently attached to the MWNT surface enhanced the interface adhesion between the MWNTs and PBT matrix and, thus, improved the compatibility. The morphologies of the nanocomposites were observed by field emission scanning electron microscopy and transmission electron microscopy, which showed that the nanotubes were homogeneously dispersed in the PBT matrix when the MWNT content was lower than 0.75 wt %. Differential scanning calorimetry and thermogravimetric analysis were used to investigate the thermal properties of the nanocomposites. The results indicate that the MWNTs acted as nucleation sites in the matrix, and the efficiency of nucleation was closely related to the dispersion of the MWNTs in the matrix. Additionally, the thermal stability of PBT was improved by the addition of the MWNTs. © 2010 Wiley Periodicals, Inc. J Appl Polym Sci 118: 2929–2938, 2010

Key words: compatibilization; dispersions; ring-opening polymerization

INTRODUCTION

Carbon nanotubes (CNTs) have attracted tremendous attention because of their unique combination of electronic, mechanical, chemical, and thermal properties[1–3] since a landmark article in 1991 was published by Iijima.[4] Those properties make CNTs excellent candidates as advanced filler materials in nanocomposites. However, the achievement of a homogeneous dispersion and good interfacial bonding between the CNTs and polymer matrix is the main challenge because of the strong van der Waals forces between individual tubes, which often lead to agglomeration, bundling together, and entanglement[5] and, thus, reduce the expected properties of the resulting nanocomposites. It is well known that the material properties of a nanocomposite invariably depend on the strength of specific interactions between the CNTs and the matrix polymer.[6,7] Therefore, the compatibility between polymers and nanotubes has been envisaged as a very important factor affecting the properties of CNT–polymer composites. Recently, various strategies have been reported for the modification of the compatibility between nanotubes and polymer matrices; these have involved covalent or noncovalent attachments of functional groups or long polymer chains to the CNT surface. Noncovalent functionalization methods, such as polymer wrapping and π-π stacking on the surface of CNTs, are difficult to correlate quantitatively with properties attributable to the presence of excess polymer and the slippage of stacked molecules.[8,9] However, the covalent approach allows for the formation of a strong interface between the nanotubes and the polymer matrix due to strong chemical bonding of the polymer molecules to the CNT surface. Particularly attractive is the use of polymers in nanotube functionalization that are either identical to or structurally altered from the matrix polymers; these, thus, ensure full compatibility in the resulting nanocomposites. Furthermore, covalent functionalization can provide a method for engineering the nanotube–polymer interface for optimal composite properties. *In situ* polymerization in the presence of CNTs has been intensively explored for the preparation of polymer-grafted nanotubes and the processing of the corresponding polymer composite

Correspondence to: G. Yang (ygs@geniuscn.com).

materials. The main advantage of this method is that it enables the grafting of polymer macromolecules onto the convex walls of the CNTs; this provides better nanotube dispersion and high nanotube contents. Yan and Yang[10] prepared polyamide 6–multiwalled carbon nanotubes (MWNTs) nanocomposites by this approach, taking toluene 2,4-diisocyanate functionalized MWNTs as activators for the anionic ring-opening polymerization of ε-caprolactam. Kong et al.[11] successfully functionalized MWNTs with various contents of poly(methyl methacrylate) layers by *in situ* atom transfer radical polymerization grafting polymerization. Zhou and coworkers[12,13] prepared oligohydroxyamide-functionalized MWNTs for nanotube–poly(*p*-phenylene benzobisoxazole) composites. Lin et al.[14] synthesized polymer-grafted CNTs based on acylated CNTs with poly(vinyl alcohol) and found that the poly(vinyl alcohol)–CNT nanocomposites were of high optical quality without any observable phase separation. Among the aforementioned nanocomposites, the combination of *in situ* polymerization and chemical graft functionalization of CNTs by the matrix polymer was an effective way for achieving homogeneous dispersion for high-performance polymer/CNT nanocomposites.

Recently, cyclic butylene terephthalate (CBT) oligomers have aroused considerable interest because of their waterlike viscosity and ability to be rapidly polymerized to form the engineering thermoplastic poly(butylene terephthalate) (PBT). In this study, we introduced functionalized MWNTs to prepare PBT/MWNT nanocomposites by the *in situ* approach. First, a novel cyclic initiator containing Sn—O bonds was covalently attached to the MWNT surface. The Sn—O bond has been shown to be an active polymerization site for the polymerization of lactones and cyclocarbonates according to a coordination–insertion mechanism.[15–19] Afterward, the immobilized initiators on the nanotube surface initiated the ring-opening polymerization of CBT to form the polymer molecules bound to the nanotube. We expected that the grafted PBT could act as an *in situ* compatibilizer in the nanocomposites, which could result in the homogeneous dispersion of the MWNTs in the PBT matrix. Therefore, the dispersion of MWNTs in the PBT matrix was studied with field emission scanning electron microscopy (FESEM) and transmission electron microscopy (TEM). Additionally, the effect of the MWNTs on the thermal properties of PBT in the nanocomposites was also explored in detail.

EXPERIMENTAL

Materials

Carboxyl-functionalized multiwalled carbon nanotubes (MWNT–COOHs) were purchased from Chengdu Organic Chemistry Co., Ltd. (Chengdu, China). The diameter of the MWNTs was about 10–20 nm, and the content of —COOH was around 2.0 wt %. CBT oligomers (CBT 100) and butyl tin chloride dihydroxide were purchased from Cyclics Corp. (New York). Thionyl chloride ($SOCl_2$), 1,4-butanediol, and dibutyl tin oxide were provided by Shanghai Chemical Reagent Corp. (Shanghai, China) and were used without further purification. Other solvents were all analysis grade and were used as received unless otherwise specified.

Preparation of the multiwalled carbon nanotube supported initiator (MWNT–Sn)

Hydroxyl-functionalized multiwalled carbon nanotubes (MWNT–OHs) were prepared according to the method reported by Yan et al.[20] Briefly, the MWNT–COOHs were reacted with excess $SOCl_2$ and then excess glycol. The raw MWNT–OHs were collected by filtering and washing with anhydrous tetrahydrofuran (THF) and were then dried *in vacuo*. Then, the dried MWNT–OHs (1 g) and dibutyl tin(IV) oxide (54 mg, 21.7 mmol) were added to 150 mL of dry toluene contained in a three-necked flask equipped with a Dean–Stark moisture trap. The mixture was held at reflux until no more water collected in the trap. The solid was separated by filtration and washed with anhydrous THF several times. The raw product was extracted by ethyl acetate to remove any possible adsorbed dibutyl tin(IV) oxide for 12 h to guarantee that the MWNT–Sn's were as pure as possible. Finally, the MWNT–Sn's were dried *in vacuo* at 60°C for 8 h. The reaction process is described in Scheme 1.

Preparation of the PBT/MWNTs nanocomposites

The desired amount of MWNT–Sn was added to a solution of 30 g of CBT and 150 mL of THF, and a stable suspension was obtained with the aid of ultrasonication for 1 h at room temperature. Most of the THF was evaporated *in vacuo* at 50°C, and then, the black mixture was heated to 200°C *in vacuo* for another 30 min to remove trace amount of THF. Afterward, appropriate amount of butyl tin chloride dihydroxide was added to ensure that the contents of the initiator in all preparations were identical. The whole procedure was completed within 30 min under mechanical stirring at a speed of 500 rpm. According to the content of the MWNTs (weight percentage), the nanocomposites were identified as PBT/MWNT-0.5, PBT/MWNT-0.75, PBT/MWNT-1.0, and PBT/MWNT-1.5.

As a comparison, a PBT/MWNT composite with 0.75 wt % MWNTs was also prepared by the aforementioned method. The difference was that MWNT–COOH took the place of MWNT–Sn. The composite

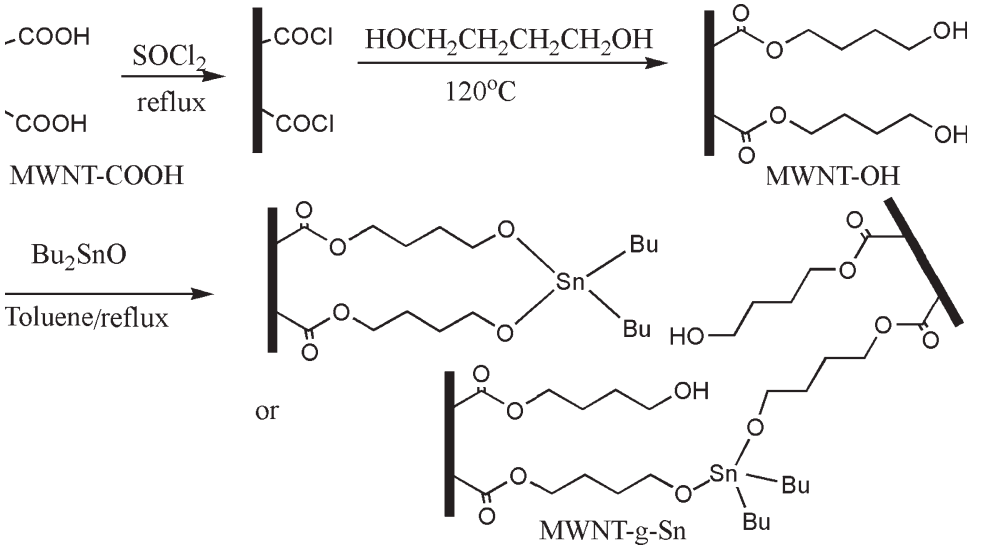

Scheme 1 Preparation of MWNT–Sn.

was identified as PBT/MWNT–PM0.75 (where PM indicates physical mixing and 0.75 indicates the content of the MWNTs (weight percentage)).

Separation of the poly(butylene terephthalate)-grafted multiwalled carbon nanotubes (MWNT–PBTs)

Typically, a sample of PBT/MWNT-0.75 was dissolved in a trifluoroacetic acid/trichloromethane (1 : 3, v/v) solvent mixture under stirring overnight at room temperature. After this, the suspension was separated by filtration and then washed with methanol. The dispersing, filtering, and washing cycle was repeated several times to remove ungrafted polymer. Finally, the obtained MWNT–PBTs were dried in a vacuum oven at 80°C for 24 h. In addition, the homo-poly(butylene terephthalate) (homo-PBT) was precipitated in excess methanol from the collected filter, washed thoroughly with methanol, and finally, dried *in vacuo* at 80°C for 24 h. The recovered polymer was prepared for viscosity measurement.

Characterization

The intrinsic viscosity ([η]) of the samples dissolved in 0.5 g/dL concentrated mixture solvent of phenol/1,1,2,2-tetrachloroethane(w/w = 60 : 40) was determined with an Ubbelohde viscometer (Shanghai, China) thermostated at 30 ± 0.5°C in a water bath. The measurements were carried out at only one specific concentration according to the single-point method.[21]

Fourier transform infrared (FTIR) spectra in KBr pellets were recorded on a Nicolet Avater-360 spectrometer (Madison, Wisconsin), and the nuclear magnetic resonance (NMR) spectra of the MWNT–PBTs in CF_3COOD were measured with a Bruker ARX 400-MHz spectrometer (Billerica, MA) with tetramethylsilane as an internal standard. X-ray photoelectron spectroscopy was conducted on a Thermo Escalab 250 system (Waltham, UK) with Al Kα radiation. Field emission transmission electron microscope (FETEM) (JEM-2100F (Tokyo, Japan)) was used to observe the nanostructures of the MWNT–COOHs and MWNT–PBT. Both TEM (Hitachi H-800 (Tokyo, Japan)) and FESEM (JEOL 6700F (Tokyo, Japan)) were used to observe the dispersion of the MWNTs in the nanocomposites.

Differential scanning calorimetry (DSC) measurements were carried out on a PerkinElmer Diamond DSC instrument (Shelton, CT) equipped with a liquid subambient accessory and calibrated with In standards. The samples were heated to 250°C at a rate of 20°C/min under an N_2 atmosphere from room temperature and held at 250°C for 5 min to erase any previous thermal history. Then, they were cooled to 50°C at a cooling rate of 10°C/min to obtain the crystallization temperature (T_c). Finally, they were reheated to 250°C at a heating rate of 10°C/min. The melting temperature (T_m) and T_c were taken as the endothermal and exothermal phenomena, respectively, in the DSC curves. Repeated measurements on each sample showed excellent reproducibility.

The degree of crystallinity (X_c) for the PBT and PBT/MWNT nanocomposites was calculated from the enthalpy evolved during crystallization on the basis of the cooling scans with the following equation:

$$X_c(\%) = \frac{\Delta H_m}{\Delta H_m^o} \times 100 \quad (1)$$

where ΔH_m is the measured heat of fusion for the sample and ΔH_m^o is the heat of fusion of a 100% crystalline polymer. According to previous studies, the heat of fusion of 100% crystalline PBT is 140 J/g.[22]

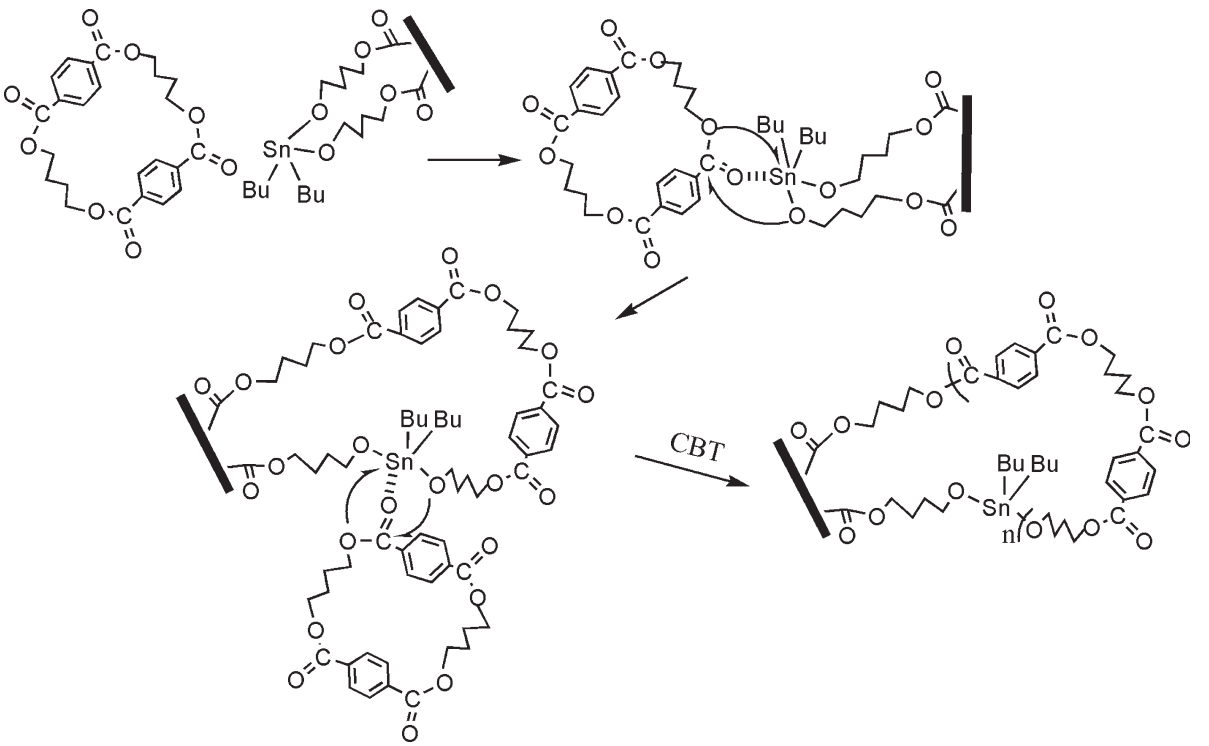

Scheme 2 Coordination–insertion mechanism of the ring-opening polymerization of CBT.

Thermogravimetric analysis (TGA) was performed with a SDT Q600 (TA Instruments Corp., New Castle, DE). All of the samples were heated from 50 to 600°C at a heating rate of 10°C/min in a nitrogen atmosphere.

RESULTS AND DISCUSSION

Characterization of the MWNT–PBTs

The objective of this study was to take advantage of the ring-opening polymerization of CBT initiated by MWNT–Sn. As shown in Scheme 2, the polymerization proceeded via an acyl–oxygen cleavage of the CBT with insertion of the monomer into the metal–oxygen bond of the initiator. First, the monomer formed a complex with the initiator through interactions between the carbonyl group of CBT and the metal atom; this was followed by the ring opening of the CBT, which occurred via cleavage of the acyl–oxygen bond. Afterward, the hydroxyl group of butyl tin chloride dihydroxide terminated the active macrorings and resulted in a linear polymer.

Both ^{1}H-NMR and ^{13}C-NMR were used to confirm the chemical structure of the MWNT–PBT copolymer, and the results are illustrated in Figure 1. The corresponding proton peaks of the grafted PBT chains appeared in the ^{1}H-NMR spectrum of MWNT–PBT at 8.67, 5.08, and 2.60 ppm. In the corresponding ^{13}C-NMR spectrum, the carbon signals were found as peaks at 174.4, 138.9, 134.9, 71.8, and 29.8 ppm. Furthermore, as shown in Figure 2, the FTIR spectrum of MWNT–PBT was visible and quite similar to that of PBT (obtained by the ring-opening polymerization of CBT initiated by butyl tin chloride dihydroxide[23,24]). For instance, the characteristic absorptions at 1718 and 1261 cm^{-1} corresponded to the —C=O stretching

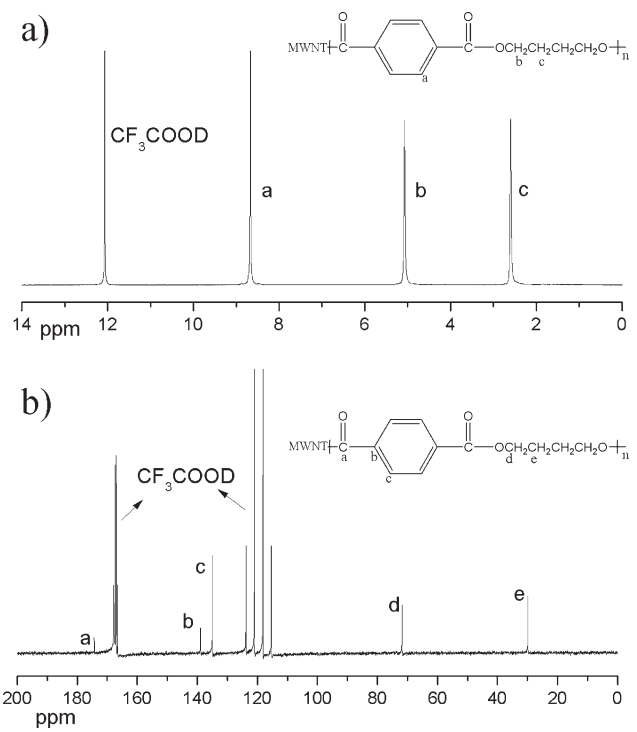

Figure 1 (a) ^{1}H-NMR and (b) ^{13}C-NMR spectra of MWNT–PBT in CF_3COOD.

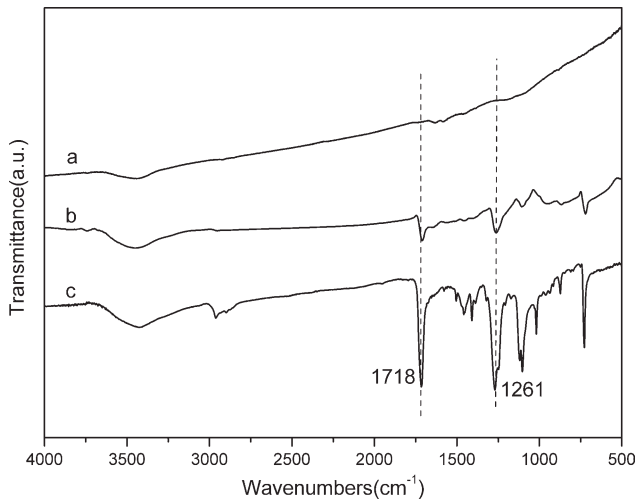

Figure 2 FTIR spectra of the (a) neat MWNT–COOHs, (b) MWNT–PBT, and (c) PBT.

vibration and the —C—O stretching vibration, respectively. In contrast, there were no visible peaks of neat the MWNT–COOHs. All of these results confirm that PBT was grafted onto the surface of the MWNTs.

To give a direct view of MWNT–PBT, FETEM was conducted to observe the nanostructures of the MWNT–COOHs and MWNT–PBTs, and the representative images are shown in Figure 3. Compared with the neat MWNT–COOHs, the MWNT–PBTs looked thicker, and the tubelike nanostructure could still be clearly observed. As shown in Figure 3(d), under high magnification, a core–shell structure with the polymer layer as the shell was observed for MWNT–PBT. Additionally, the boundary between the tube and the polymer layer became distinct because of the differing electron contrast of the MWNTs and PBT, and the average thickness of the polymer layer was about 6 nm. This result of FETEM further confirms the success of PBT grafting from the MWNT surface; this made the nanotubes more compatible with the polymer matrix.

Viscosity-average molecular weight (M_v) of some samples

To investigate the influence of the MWNTs on the molecular weight of PBT, the values of [η] for the PBT and the homo-PBT of PBT/MWNT-0.75 were calculated according to the following equation:[25]

$$[\eta] = \frac{\sqrt{2(\eta_{sp} - \ln \eta_{rel})}}{c} \quad (2)$$

where η_{sp} is specific viscosity and η_{rel} relactive viscosity. Meanwhile, M_v was obtained from the following Mark–Houwink equation:[21]

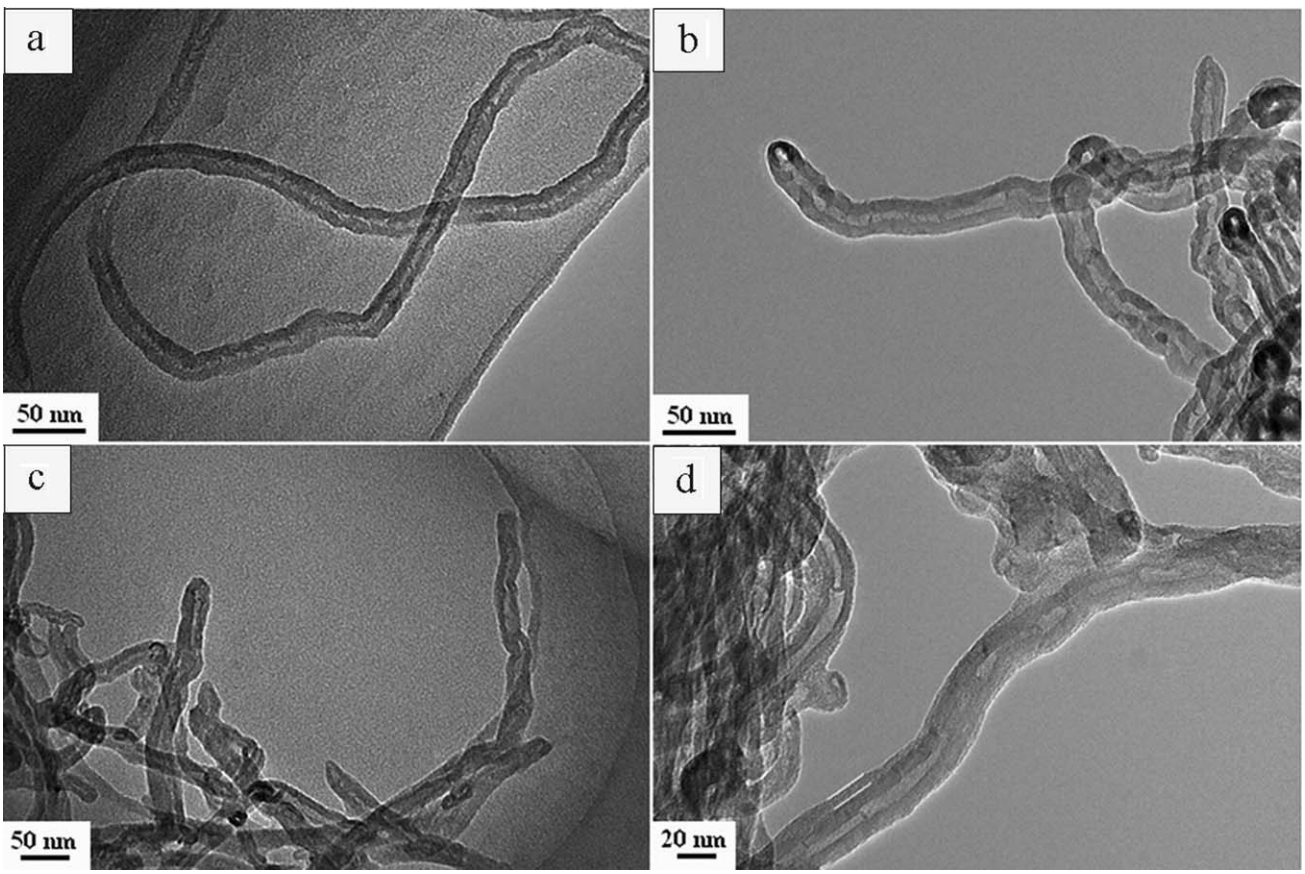

Figure 3 Representative FETEM images of the (a) neat MWNT–COOHs and (b–d) MWNT–PBT.

TABLE I
M_v Values of PBT and Homo-PBT of PBT/MWNT-0.75

Sample	[η] (dL/g)	M_v[a]
PBT	1.730	61,539
Homo-PBT	1.697	60,193

[a] Estimated from the measured [η].

$$[\eta] = 1.166 \times 10^{-4} M_v^{0.871} \quad (3)$$

The results are listed in Table I.

As shown by the values of M_v for the PBT and the homo-PBT of PBT/MWNT-0.75, the MWNTs had little influence on the M_v values of the resultant PBT in the case of the uniform molar ratio of monomer to initiator. However, the addition of MWNTs could considerably retard the process of the ring-opening polymerization; hence, the time of polymerization was set as 30 min to ensure completion.

Dispersion of the MWNTs in the nanocomposites

To investigate the effect of *in situ* compatiblization on the dispersion, FESEM and TEM were carried out to observe the dispersion of the MWNTs in the obtained nanocomposites. Figure 4 shows the FESEM images of cryogenically fractured surfaces in liquid nitrogen for the PBT/MWNT nanocomposites. Because of the MWNTs embedded in the matrix, all of the fractured surfaces were etched by NaOH/ethanol (10 wt %) for 24 h at room temperature to remove the polymer coating on the outside of the MWNTs. All samples were observed at the same magnification. As shown, the white-dot regions represented the ends of MWNTs that were stretched out of the PBT matrix. The MWNTs were homogeneously dispersed in the PBT matrix at low content. However, some aggregation of MWNTs was observed at the high content.

More direct evidence of the formation of a true nanocomposite was provided by TEM studies of ultramicrotomed sections. The TEM images in Figure 5(a,b) show, for instance, the dispersion of the MWNTs in the PBT matrix for ultrathin sections of the nanocomposites containing 0.50 and 0.75 wt % MWNTs, respectively. Generally, most of the MWNTs were homogeneously nanodispersed in the PBT matrix, although some small entanglement was observed at high magnification. To demonstrate the

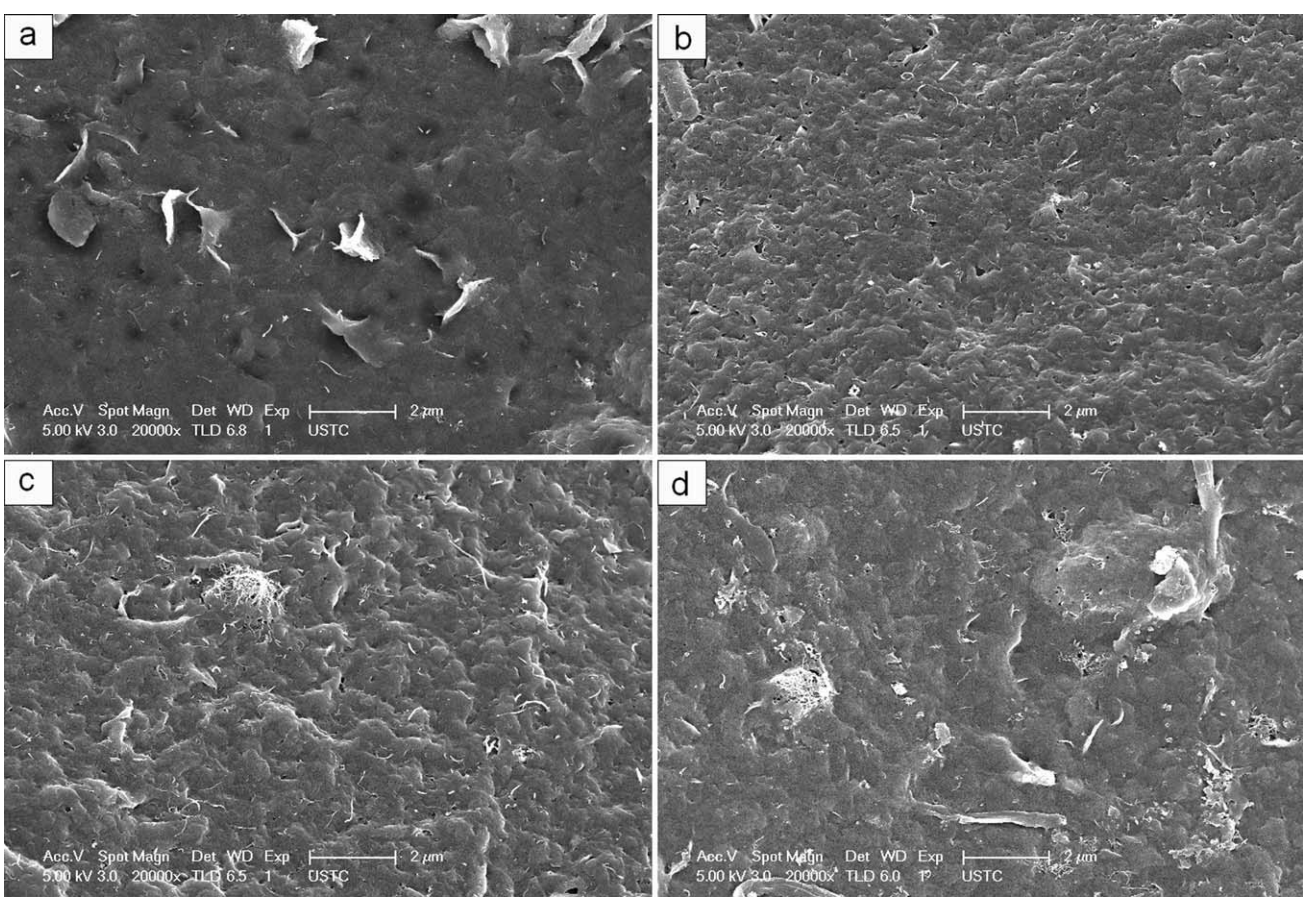

Figure 4 FESEM images of the fracture surfaces of (a) PBT/MWNT-0.5, (b) PBT/MWNT-0.75, (c) PBT/MWNT-1.0, and (d) PBT/MWNT-1.5.

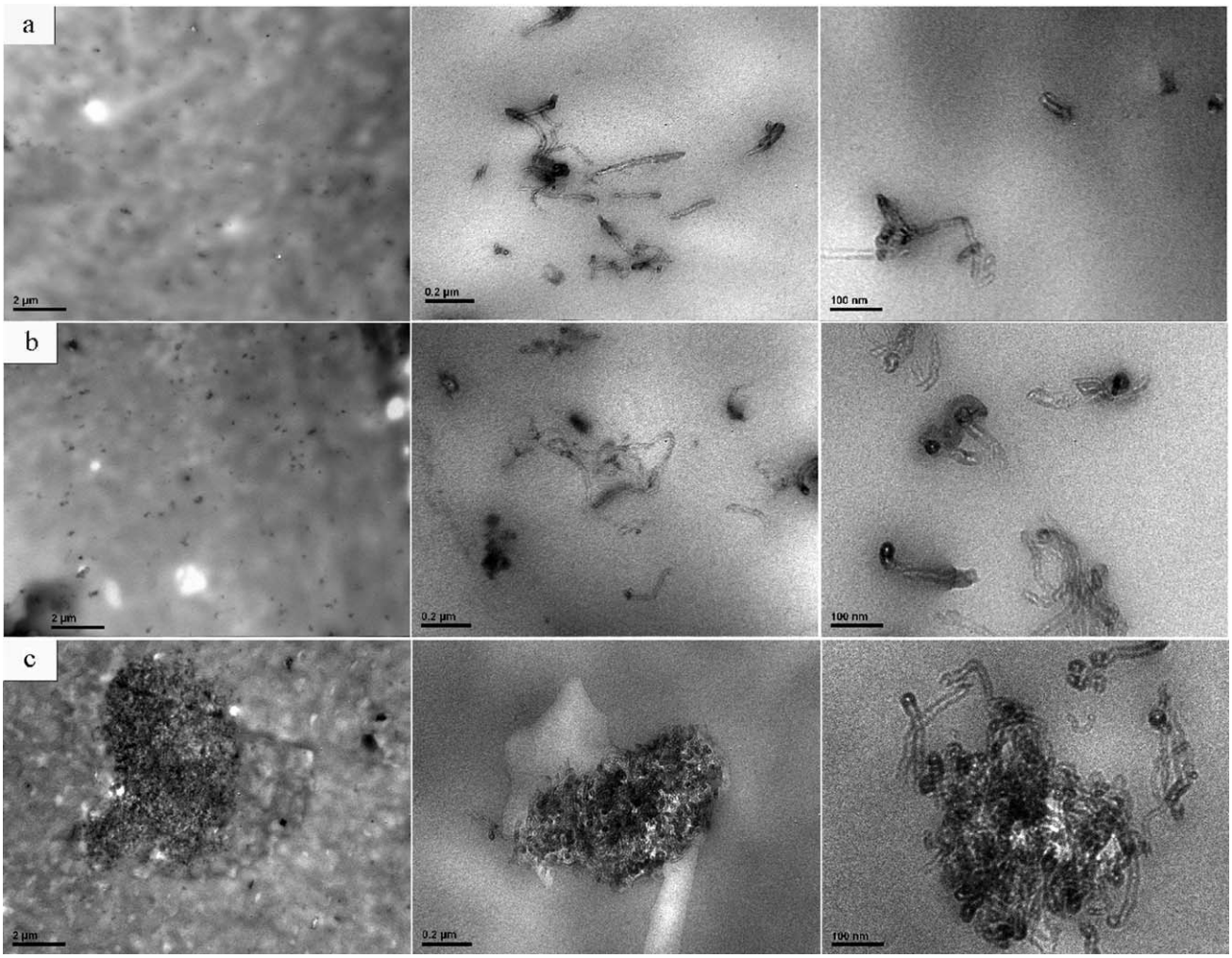

Figure 5 TEM images of (a) PBT/MWNT-0.5, (b) PBT/MWNT-0.75, and (c) PBT/MWNT–PM0.75 at different magnification.

advantage of the *in situ* compatibilization of the MWNTs with PBT, TEM images of PBT/MWNT–PM0.75 were also obtained and are shown in Figure 5(c). It was clear that large agglomerates of MWNTs existed in the composite; this indicated that a poor dispersion of MWNTs existed in the composite because of weaker interfacial adhesion between the MWNTs and PBT matrix. It is well known that MWNTs have exceptionally high aspect ratios, high surface areas, and intrinsic van der Waals attractions among tubes; this results in their significant agglomeration; thus, it was difficult to achieve homogeneous dispersion in the polymer matrix.[5] On the other hand, the nonreactive surface of the MWNTs led to weaker interfacial adhesion with the polymer matrix; this implied aggregation and entanglement. In this study, the newly synthesized MWNT–Sn's were used directly to prepared PBT–MWNT nanocomposites; in this way, the compatibility between the PBT and MWNTs was significantly improved by the *in situ* formed compatibilizer. The polymer molecules covalently grafted onto the MWNTs improved the compatibilization between the nanotubes and polymer matrix. This tended to dramatically promote the nanotube dispersion and, hence, further improved the nanocomposite properties. Because of the poor dispersion of MWNTs in the PBT/MWNT–PM0.75 composites, no further characterization was carried out in this study.

Crystallization and melting behavior

It is well known that the dispersion of MWNTs in a matrix can be deduced from the changes in T_m and T_c of the polymer matrix as well. Therefore, the effect of the MWNTs on the melting and crystallization behavior of the PBT was investigated by DSC, and the results are illustrated in Figure 6 and Table II. It is well established that the thermal behavior of a polymer is affected by its previous thermal history, and thus, all of the samples were subjected to the same thermal treatments.

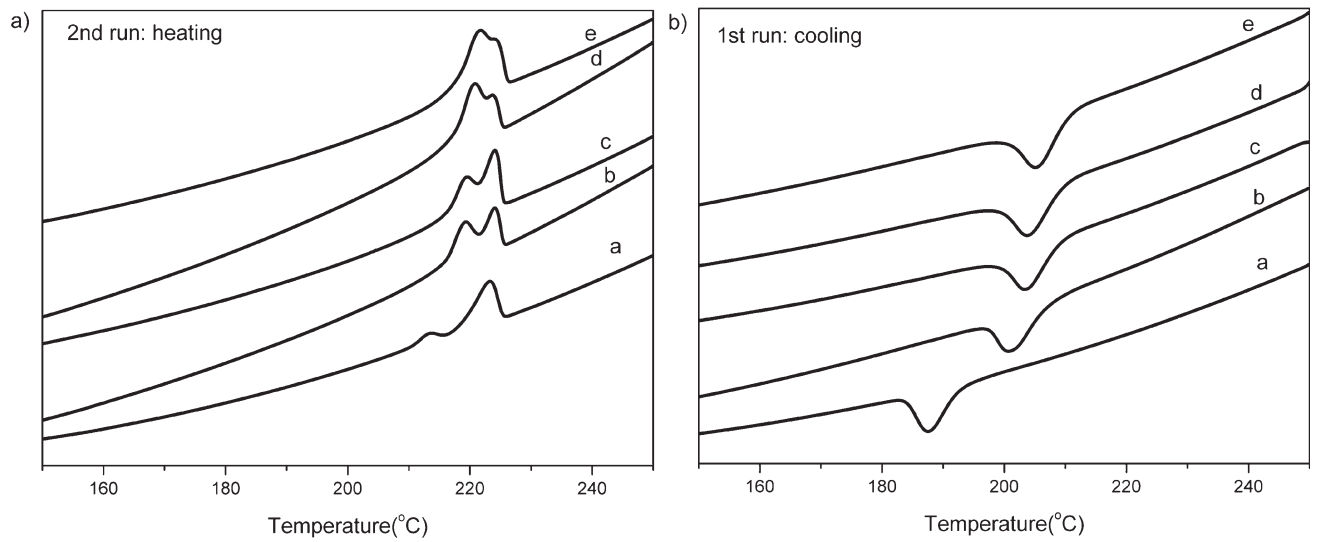

Figure 6 DSC curves for the (a) PBT, (b) PBT/MWNT-0.5, (c) PBT/MWNT-0.75, (d) PBT/MWNT-1.0, and (e) PBT/MWNT-1.5.

As shown in Figure 6(a), all of the samples exhibited double melting peaks during the second heating scan; this was characteristic phenomena for PBT when obtained by the *in situ* polymerization of CBT.[26,27] Generally, for many thermoplastic polyesters, multiple endotherm peaks can observed because of the presence of two or more groups of crystals with different morphologies.[28–31] They can be caused by remelting–recrysallization processes during DSC scanning.[32–35] In this study, the lower one represented the melting of imperfect or smaller/thinner crystals, and the higher one represented bigger crystallites. The melting peak located at the low temperature (T_{mI}) increased and that at the higher temperature (T_{mII}) gradually decreased as the content of the MWNTs increased. This may have been due to the fact that the MWNTs as heterogeneous nucleating agents accelerated the crystallization rate. However, the mobility of the PBT chains was also restricted by the covalent links between the PBT and MWNTs; this resulted in more imperfect or smaller/thinner crystallites. In addition, with increasing content of MWNTs, the area of lower temperature was larger, whereas the higher one nearly disappeared. Moreover, the value differences between T_{mI} and T_{mII} became smaller as with more MWNTs. This was attributed to the fact that the double melting behavior of the filled PBT samples was much less pronounced than that of PBT, which may have been due to the broadening and overlapping of individual melting peaks typical for polymers when fillers are present.[36]

During the cooling scan, only one crystallization peak was observed for all of the samples. The single crystallization peak indicated that a single-mode distribution in the crystallization size was formed during the cooling process. For PBT, the crystallization peak temperature was 187.7°C. However, T_c increased up to 201.3°C when the content of MWNTs was 0.5 wt %, 13.6°C higher than that of PBT. For the nanocomposites with 0.75, 1.0, and 1.5 wt %, the T_c values were 203.9, 204.5, and 205.3°C, respectively, in the cooling scans. These results suggest that the MWNTs acted as good nucleating reagents for PBT and accelerated the rate of crystallization greatly. However, with increasing MWNT content, the nucleating efficiency decreased, although T_c kept increasing. Similar results were reported previously in other articles.[37–39] The major factor that could affect the nucleating efficiency was the dispersion of the MWNTs in the PBT matrix. When the content of the MWNTs increased, aggregation inevitably happened, and thus, the effective nucleation sites provided by the MWNTs may have

TABLE II
DSC Data of the PBT and PBT/MWNT Nanocomposites

Sample	MWNT content (wt %)	T_{mI}/T_{mII} (°C)	T_c (°C)	ΔH_{mI+II}* (J/g)	ΔH_c* (J/g)	X_c (%)
PBT	0	213/223	187.7	20.26	−24.20	14.4
PBT/MWNT-0.5	0.5	219/224	201.3	37.00	−32.79	26.4
PBT/MWNT-0.75	0.75	219/224	203.9	40.46	−33.63	28.9
PBT/MWNT-1.0	1.0	221/224	204.5	41.42	−33.42	29.6
PBT/MWNT-1.5	1.5	222/224	205.3	41.98	−33.09	30.0

* ΔH_{mI+II} indicates the combination of the low and the high melting enthalpy. ΔH_c indicates the crystallization enthalpy.

decreased. X_c, calculated according to eq. (1), is listed in Table II, too. As shown in Table II, it was evident that additions of the MWNTs did increase X_c of PBT, and the values of X_c of the nanocomposites had a nearly twofold increase compared to that of PBT.

Thermal stability

Figure 7 illustrates the thermogravimetric curves of the same samples in nitrogen, from which the temperature of initial thermal decomposition (T_i), the temperature corresponding to the maximum weight loss rate (T_{max}), and the residue at 550°C were determined; the values obtained are collected in Table III. Many studies have reported that the thermal properties of a polymer can be improved significantly by the incorporation of a only small amount of CNTs. This improvement is mainly attributed to three aspects: good matrix–nanotube interaction, nice thermal conductivity of the nanotubes, and also, their barrier effect.[40] However, hardly any remarkable change in the decomposition was observed apart from thermally stable residue, which corresponded well with the nanotube content. Similar phenomena have been also observed in polycaprolactone/MWNT,[40] poly(ethylene terephthalate)/MWNT,[41] and polyamide 6/MWNT[42] nanocomposites. It is accepted that the thermal degradation of polyester is led by random chain scission or specific chain-end scission. In our case, there may have been some residual carboxyl groups on the MWNT surface, which promoted the degradation of the polymer matrix.[36] The presence of MWNTs could have increased the thermal stability because of their nice thermal conductivity and barrier effect, whereas those residual carboxyl groups facilitated the thermal degradation of the PBT matrix, more or less.[43] Therefore, the dual effects of MWNTs made the MWNTs in the PBT matrix act merely as inertlike fillers with respect to thermal decomposition.

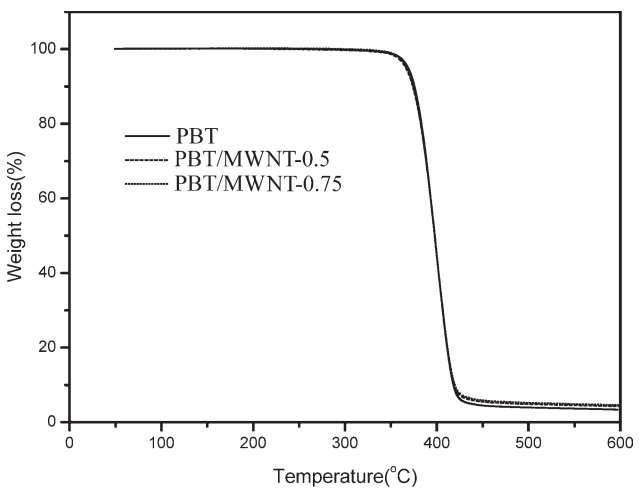

Figure 7 TGA curves of some PBT/MWNT nanocomposites (the curves of PBT/MWNT-1.0 and PBT/MWNT-1.5 are not listed because they were too close to be illustrated).

TABLE III
TGA Data of the PBT and PBT/MWNT Nanocomposites

Sample	T_i (°C)	T_{max} (°C)	Residue at 550°C (%)
PBT	377.3	398.8	3.66
PBT/MWNT-0.5	377.5	401.2	4.56
PBT/MWNT-0.75	376.8	400.2	4.89
PBT/MWNT-1.0	377.9	397.9	4.98
PBT/MWNT-1.5	377.2	398.5	5.05

CONCLUSIONS

PBT/MWNT nanocomposites were prepared through the *in situ* polymerization and *in situ* compatibilization approach. Through the attachment of the initiator to the MWNTs, PBT long-chain molecules were grafted onto the MWNT surfaces, and thus, the resulting products (MWNT–PBTs) could act as compatibilizers for the nanocomposites. The dispersion of the MWNTs in the PBT matrix was characterized by FESEM and TEM. The results reveal that the MWNTs were homogeneously dispersed in the PBT matrix when the content of MWNTs was lower than 0.75 wt %. Additionally, the presence of MWNTs significantly promoted the crystallization rate of PBT because of heterogeneous nucleation. Meanwhile, the lower T_m shifted to a high temperature, and the area of the lower T_m became larger. The effectiveness of crystallization promotion was inconspicuous as the content of MWNTs was increased. This may have resulted from the balance between the heterogeneous nucleation effect and the confined crystallization effect formed at high MWNT contents. Finally, the thermal stability of PBT was improved by the addition of the MWNTs as well.

References

1. Dresselhaus, M. S.; Dresselhaus, G.; Eklund, P. C. Science of Fullerenes and Carbon Nanotubes; Academic: New York, 1996.
2. Salvetat, J.-P.; Bonard, J.-M.; Thomson, N. H.; Kulik, A. J.; Forró, L.; Benoit, W.; Zuppiroli, L. Appl Phys A 1999, 69, 255.
3. Treacy, M. M. J.; Ebbesen, T. W.; Gibson, T. M. Nature 1996, 381, 678.
4. Iijima, S. Nature 1991, 354, 56.
5. Ebbesen, T. Carbon Nanotubes: Preparation and Properties; CRC: New York, 1997.
6. Song, Y. S.; Youn, J. R. Carbon 2005, 43, 1378.
7. Cadek, M.; Coleman, J. N.; Ryan, K. P.; Nicolosi, V.; Bister, G.; Fonseca, A.; Nagy, J. B.; Szostak, K.; Béguin, F.; Blau, W. J. Nano Lett 2004, 4, 353.

8. Chen, R. J.; Zhang, Y.; Wang, D.; Dai, H. J Am Chem Soc 2001, 123, 3838.
9. Sengupta, R.; Ganguly, A.; Sabharwal, S.; Chaki, T. K.; Bhowmick, A. K. J Mater Sci 2007, 42, 923.
10. Yan, D. G.; Yang, G. S. J Appl Polym Sci 2009, 112, 3620.
11. Kong, H.; Gao, C.; Yan, D. Y. J Am Chem Soc 2004, 126, 412.
12. Zhou, C. J.; Wang, S. F.; Zhang, Y.; Zhuang, Q. X.; Han, Z. W. Polymer 2008, 49, 2520.
13. Zhou, C. J.; Wang, S. F.; Zhuang, Q. X.; Han, Z. W. Carbon 2008, 46, 1232.
14. Lin, Y.; Zhou, B.; Fernando, K. A. S.; Liu, P.; Sun, Y. P. Macromolecules 2003, 36, 7199.
15. Kricheldorf, H. R.; Lee, S. Macromolecules 1995, 28, 6718.
16. Kricheldorf, H. R.; Lee, S.; Bush, S. Macromolecules 1996, 29, 1375.
17. Kricheldorf, H. R.; Lee, S. Macromolecules 1996, 29, 8689.
18. Kowalski, A.; Libiszowski, J.; Duda, A.; Pencaek, S. Macromolecules 2000, 33, 1964.
19. Kowalski, A.; Duda, A.; Penczek, S. Macromolecules 2000, 33, 689.
20. Kong, H.; Gao, C.; Yan, D. Y. Macromolecules 2004, 37, 4022.
21. Borman, W. F. H. J Appl Polym Sci 1978, 22, 2119.
22. Illers, K. H. Colloid Polym Sci 1980, 258, 117.
23. Brunelle, D. J.; Bradt, J. E.; Serth-Guzzo, J.; Takekoshi, T.; Evans, T. L.; Pearce, E. J.; Wilson, P. R. Macromolecules 1998, 31, 4782.
24. Tripathy, A. R.; Elmoumni, A.; Winter, H. H.; MacKnight, W. J. Macromolecules 2005, 38, 709.
25. Solomon, O. F.; Ciutâ, I. Z. J Appl Polym Sci 1992, 6, 683.
26. Mohd Ishak, Z. A.; Shang, P. P.; Karger-Kocsis, J. J Thermal Anal Calorim 2006, 84, 637.
27. Lehmann, B.; Karger-Kocsis, J. J Thermal Anal Calorim 2009, 95, 221.
28. Hybart, F. J.; Platt, J. D. J Appl Polym Sci 1967, 11, 1449.
29. Bassett, D. C.; Olley, R. H.; Raheil, I. A. M. Polymer 1988, 29, 1745.
30. Kim, H. G.; Mandelkern, L. J Polym Sci Part A-2 1972, 10, 1125.
31. Bell, J. P.; Slade, P. E.; Dumbleton, J. H. J Polym Sci Part A-2: Polym Phys 1968, 6, 1773.
32. Lee, Y.; Porter, R. S.; Lin, J. S. Macromolecules 1989, 22, 1756.
33. Radusch, H.-J. In Handbook of Thermoplastic Polyesters; Fakirov, S., Ed.; Wiley: Weinheim, 2002.
34. Righetti, M. C.; Pizzoli, M.; Lotti, N.; Munari, A. Macromol Chem Phys 1998, 199, 2063.
35. Sweet, G. E.; Bell, J. P. J Polym Sci Part A-2: Polym Phys 1972, 10, 1273.
36. Liu, Y.; Wang, Y. F.; Gerasimov, T. G.; Heffner, K. H.; Harmon, J. P. J Appl Polym Sci 2005, 98, 1300.
37. Lee, H. J.; Oh, S. J.; Choi, J. Y.; Kim, J. W.; Han, J.; Tan, L. S.; Baek, J. B. Chem Mater 2005, 17, 5057.
38. Valentini, L.; Biagiotti, J.; Lopez-Manchado, M. A.; Santucci, S.; Kenny, J. M. Polym Eng Sci 2004, 44, 303.
39. Wu, T. M.; Chen, E. C. J Polym Sci Part B: Polym Phys 2006, 44, 598.
40. Wu, D. F.; Wu, L.; Sun, Y. R.; Zhang, M. J Polym Sci Part B: Polym Phys 2007, 45, 3137.
41. Kim, J. Y.; Park, H. S.; Kim, S. H. J Appl Polym Sci 2007, 103, 1450.
42. Schartel, B.; Pötsckke, P.; Knoll, U.; Abdel-Goad, M. Eur Polym J 2005, 41, 1061.
43. Lum, R. M. J Polym Sci Polym Chem Ed 1979, 17, 203.